ELSEVIER

Journal of Nuclear Materials 256 (1998) 155–165

journal of nuclear materials

Influence of texture and physical mixture of UO_3 and C for carboreduction of UO_3 into UO_2

F. Poncet, F. Valdivieso, M. Pijolat *

Centre SPIN, Ecole des Mines de Saint-Etienne, 158 cours Fauriel, 42023 Saint-Etienne cedex 2, France

Received 16 January 1998; accepted 9 April 1998

Abstract

The carboreduction of UO_3 into UO_2 has been studied with an excess of carbon (C/U = 3 mole ratio). The results of thermogravimetric (TG) studies, X-ray diffraction (XRD) and SEM reveal that the carboreduction depends upon the texture and the physical mixture of the precursors UO_3 and carbon. Indeed, optimal carboreduction was obtained with an improvement of UO_3 and carbon grains contacts during the reduction. The preparation of the mixture (UO_3 + 3C) has been optimised by a slight manual grinding.

1. Introduction

Uranium dioxide is currently used as an intermediate step for nuclear combustible fabrication. Uranium dioxide is usually obtained by hydrogen reduction, or sometimes by carbon monoxide reduction of uranium trioxide. Reduction was found to take place in two distinct steps [1–3]: (i) the calcination of UO_3 to U_3O_8 at 923 K, (ii) the reduction of U_3O_8 to UO_2 by hydrogen at 793 K or at 100 K less by carbon monoxide.

Uranium dioxide can be also obtained by reduction with carbon [4]. But, the control of uranium oxide stoichiometry is difficult during the conversion of (UO_3 + C) to (UO_2 + C). Indeed, parasite reactions occur during the reduction of uranium trioxide, like oxidation of carbon and a mixture of CO and CO_2 is evolved [5]. Recently, Mukerjee et al. [6] have studied the carboreduction of (UO_3 + C) microspheres. These authors proposed to overcome this problem by reducing the UO_2 at temperatures below 973 K, for which the produced gas is mainly CO_2. This reaction depends upon the experimental conditions such as temperature, sample size, geometry and partial pressure of carbon monoxide. In order to get information on the texture and the physical mixture effect for the carboreduction, we have studied in this work, two mixtures of (UO_3 + 3C): a standard sample and a ground sample.

2. Experimental

2.1. Sample preparation and characterization

Two mixtures of (UO_3 + 3C) were prepared using β-UO_3 phase and carbon. The β-UO_3 is obtained from thermal decomposition of ammonium diuranate. It contains less than 1% of nitrates and presents a specific surface area of 24.6 m^2/g, as measured by the BET method, after outgassing the sample during 2 h at 373 K. The carbon was heated during 24 h at 373 K, and its specific surface area is equal to 98.5 m^2/g.

For the first (UO_3 + 3C) preparation, the UO_3 is mixed during 2 h with the carbon in a C/U = 3 mole ratio and is stocked under argon. After outgassing during 2 h at 373 K the mixture exhibits a specific surface area of 32.2 m^2/g.

The second mixture, (UO_3 + 3C) was prepared starting from the previous mixture (UO_3 + 3C) by a slight manual grinding. The manual grinding is realized in a mortar until a homogeneous black color was obtained for all of the mixture. This mixture notated (UO_3 + 3C)*, presents the same specific surface area as the unground sample (31.8 m^2/g) after outgassing during 2 h at

* Corresponding author. Tel.: +33-4 77 42 01 52; fax: +33-4 77 42 00 00; e-mail: mpijolat@emse.fr.

0022-3115/98/$19.00
PII: S0022-3115(98)00061-0

Table 1
Results of specific surface area and porosity

	Specific surface area (m^2/g)	Diameter of particule (nm) [a]	Pore volume (cm^3/g)	Pore diameter (nm)
C	98.5	27	0.36	10–100
UO_3	24.6	31	0.054	3.8–6.0
(UO_3 + 3C)	32.2	–	0.1	3.8–6.0–35
(UO_3 + 3C)*	31.8	–	0.18	3.5–6.0–60

[a] Results deduced from relation (1).

373 K. The results of the texture of these samples are summarized in Table 1.

The specific area and pore volumes were determined from isotherm adsorption and desorption measured on a micromeritics ASAP2000 apparatus. X-ray powder diffraction spectra were recorded at room temperature on a Siemens D5000 diffractometer using nickel filtered Cu-Kα radiation. Microphotographs were obtained on a scanning electron microscope Jeol JSM 840.

2.2. Thermal analysis

Thermogravimetric (TG) studies were carried out on the Setaram TAG 24 thermal analyzer equipped with a mass spectrometer. The sensitivity of the balance was 10 μg. The temperature of the sample was measured by a Pt/Pt + Rh thermocouple. The weight loss (TG), rate of weight loss (DTG) and temperature plots were recorded. The reactions were performed under flowing helium (2 l/h) with a 5 K/min heating rate up to 1173 K. The sample size in each experiment was 28 mg. At intermediate steps and at the end of the reaction, samples were analyzed by X-ray diffraction method (XRD).

3. Results and discussion

3.1. Structural and textural characterization

The XRD pattern of the UO_3 precursor used in the mixture presents the characteristic peaks of UO_3 β phase (Fig. 1). The carbon precursor was proved to be amorphous by XRD (Fig. 2). On the XRD patterns of both mixtures of UO_3 and carbon, only the β-UO_3 phase is detected (Fig. 3), which was expected since only crystalline compounds can be identified.

Specific surface areas and pore volumes are reported in Table 1. The porosity distribution is measured from the desorption isotherm using the BJH method. Adsorption desorption isotherms of all the samples C, UO_3, (UO_3 + 3C) and (UO_3 + 3C)* are given in Fig. 4(a)–(d).

An important specific surface area is observed for carbon, 98.5 m^2/g, to which corresponds a particle diameter, D, equal to 27 nm as calculated from the following relation (assuming spherical particles):

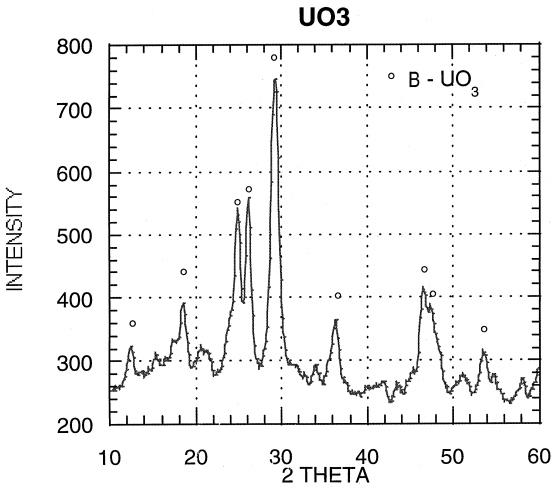

Fig. 1. The XRD pattern of UO_3.

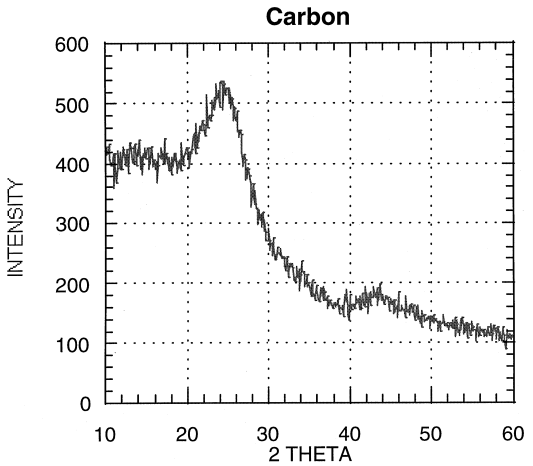

Fig. 2. The XRD pattern of carbon.

$$D = \frac{6}{\rho S} \tag{1}$$

in which ρ is the density (2.25 g/cm^3 for carbon) and S the specific surface area.

The pore size distribution of carbon shown in Fig. 5(a) presents a wide peak from 10 to 100 nm, whose

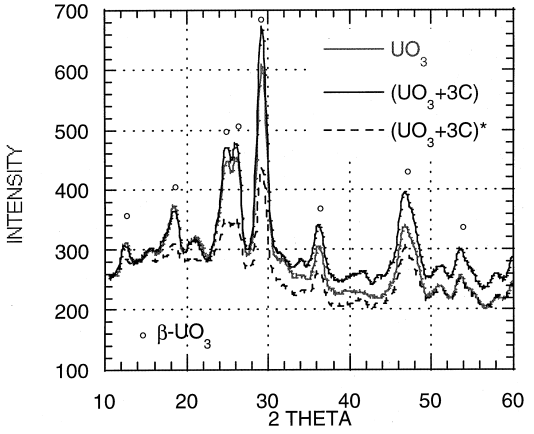

Fig. 3. The XRD pattern of UO_3, (UO_3 + 3C) and (UO_3 + 3C)*.

maximum intensity is about 0.5 cm^3/g at 40 nm. This indicates the presence of a large mesopore population with a cumulative specific pore volume equal to 0.36 cm^3/g.

For β-UO_3, the specific surface area is equal to 24.6 m^2/g which leads (using relation (1)) to a mean particle diameter of 31 nm, assuming spherical particles and density of 8 g/cm^3. The pore size distribution (Fig. 5(b)) presents two peaks centered at about 3.8 and 6.0 nm which corresponds to an intensity lower than that found with carbon. The cumulative specific pore volume is found to be equal to 0.054 cm^3/g.

In the case of the two mixtures, the specific surface area is equal to 32 ± 2 m^2/g (which agrees with the value 32.6 m^2/g calculated from the specific surface areas of the two UO_3 and C powders), but the pore size distributions are quite different (Fig. 5(c) and (d)). The pore size distribution found for (UO_3 + 3C) is similar to that of the UO_3 compound, since the mass of carbon used in the mixture gives a contribution of only 12%. However, if we take into account the cumulative pore volumes relative to each compound, we obtain a calculated cumulative pore volume for the mixture equal to 0.09 cm^3/g, which is in very good agreement with the measured one (0.1 cm^3/g).

For the ground mixture, we observe, besides the bimodal porosity due to UO_3, the appearance of a large peak centered at about 60 nm. This is clearly illustrated in Fig. 6, in which the UO_3 and carbon pore size distributions have been reploted using a specific volume scale related to that of the corresponding amount in the mixture, which allows a direct comparison of the various peak intensities. These new pores cannot be attributed to the carbon, because the peak intensity is too high and the pore size is too large compared to what can be expected from Fig. 5(a). In order to understand the origin of this new porosity, the two mixtures were observed by SEM.

The mixtures observed at the same magnification (×50) and shown in Figs. 7 and 8 present different sizes of particles. On one hand, for the standard (UO_3 + 3C) mixture (Fig. 7), we observed only few particles in 200 μm size of diameter. On the other hand, for the ground mixture (UO_3 + 3C)* many particles inferior to 100 μm size of diameter are observed in Fig. 8. If we compare the two mixtures at higher magnification (×1000) in Figs. 9 and 10, we can see only the surface of an agglomerate for the unground mixture (UO_3 + 3C) (Fig. 9). We can see black and white particles. A microanalysis X in these regions confirms the presence of carbon for dark particles and uranium for white particles. In the ground mixture (UO_3 + 3C)*, Fig. 10, we can observe entire particle, whose size is 10–40 μm in diameter.

So, according to the BET and porosity results and these observations, we can represent the two mixtures by the schemes given in Figs. 11 and 12. The mixture (UO_3 + 3C) represented in Fig. 11 shows large agglomerates (200 μm diameter) of smaller aggregates (10 μm diameter) of UO_3 elementary particles (0.03 μm diameter), all of them being overlapped by carbon grains.

Such a description accounts for the pore size distribution, cumulative pore volumes, and specific surface area of the powder, all the elementary particles are accessible to the nitrogen during adsorption measurement.

The ground mixture (UO_3 + 3C)* is represented in Fig. 12 by new agglomerates (30–40 μm diameter) of the previous aggregates (10 μm diameter) of UO_3 particles, however this time carbon grains are located inside the agglomerates, directly in contact with the UO_3 aggregates. These new contacts between carbon and uranium trioxide aggregates created by the grinding is certainly at the origin of the formation of the porosity observed at 60 nm (Fig. 5(d)).

In conclusion, the grinding of the mixture (UO_3 + 3C) has broken the large agglomerates of uranium trioxide aggregates and has enabled the penetration of the carbon inside the agglomerates, and finally has increased the number of contacts between carbon grains and uranium oxide aggregates. Nevertheless, this rearrangement has not changed the surface accessible to the gas (same specific surface area for both samples) because the manual grinding does not modify the size of the elementary particles.

3.2. Thermal analysis

3.2.1. Thermal reduction of β-UO_3

Fig. 13 presents the weight loss (TG) and rate of weight loss (DTG) curves during β-UO_3 heating. An initial weight loss (less than 1 wt%) around 373 K is observed, accompanied by an evolution of water as indicated by the appearance of mass 18 at the mass spectrometer. This is due to the desorption of water contained in the sample. We can also see an important

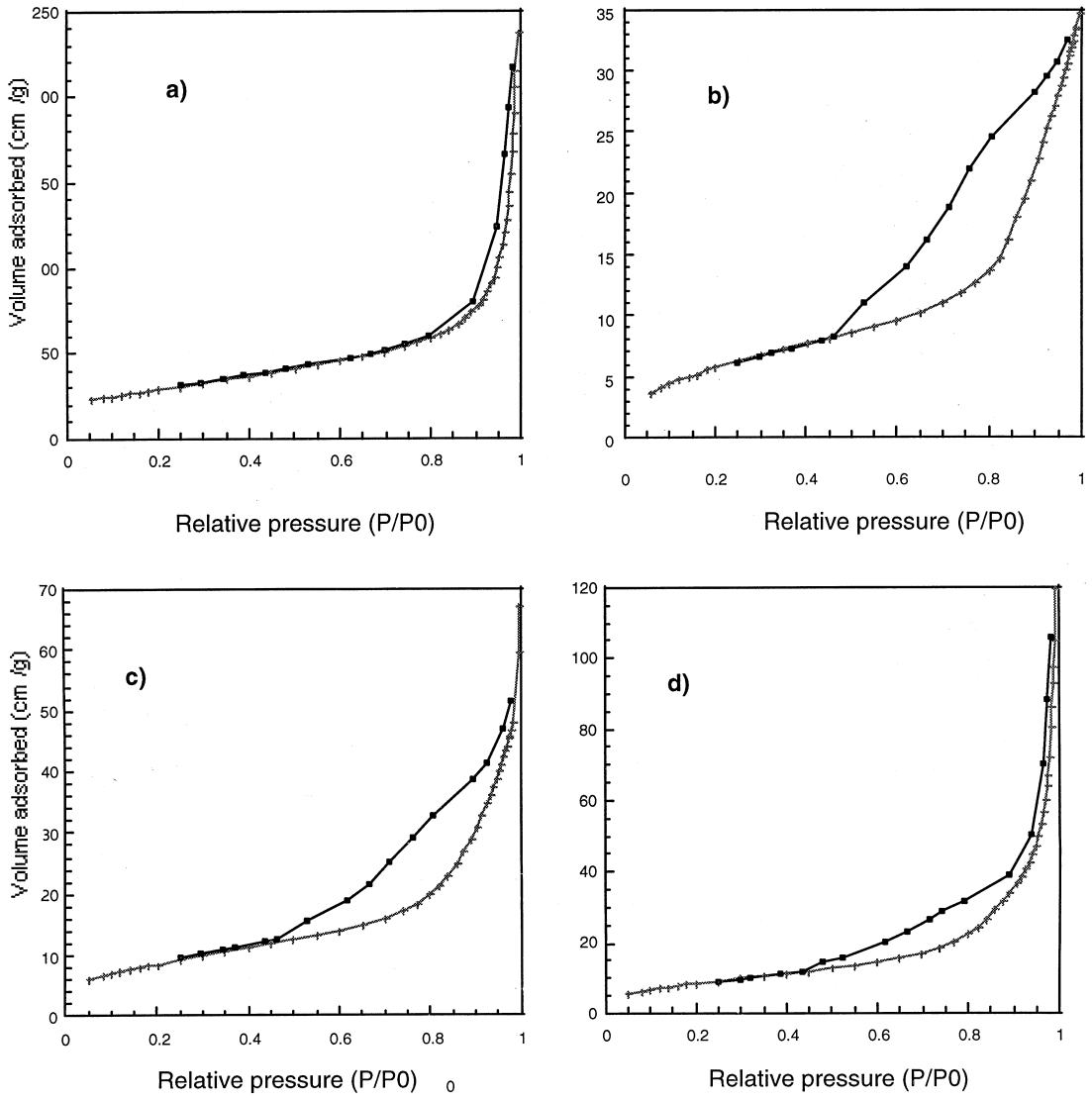

Fig. 4. Adsorption desorption isotherms of (a) carbon, (b) uranium trioxide, (c) (UO_3 + 3C) and (d) (UO_3 + 3C)* ground mixture.

weight loss (1.86 wt%) with a DTG peak at 823 K accompanied by an important emission of oxygen (appearance of mass 32 to the mass spectrometer). This weight loss corresponds exactly to the theoretical weight loss according to the thermal decomposition of UO_3 into U_3O_8 following the reaction (2):

$$3UO_3 \rightarrow U_3O_8 + \frac{1}{2}O_2. \quad (2)$$

The X-ray powder pattern taken on a heated sample confirmed the formation of U_3O_8 compound. Consequently, the DTG peak at 823 K is attributed to the transformation of UO_3 into U_3O_8 by thermal decomposition.

3.2.2. Carboreduction of (UO_3 + 3C) and (UO_3 + 3C) ground*

The TG and DTG curves for the two mixtures of UO_3 and carbon, unground and ground, during heating up to 1200 K are presented respectively in Figs. 14 and 15.

Four DTG peaks are observed for the undground mixture at 373, 713, 823 and 863 instead of three DTG peaks at 373, 713 and 863 K for the ground mixture. The first one at 373 K, is observed for both mixtures, with a weight loss inferior to 1% and accompanied to an emission of water, which can be attributed to the loss of adsorbed water, as for the β-UO_3 compound. All the other DTG peaks observed for the two mixtures are

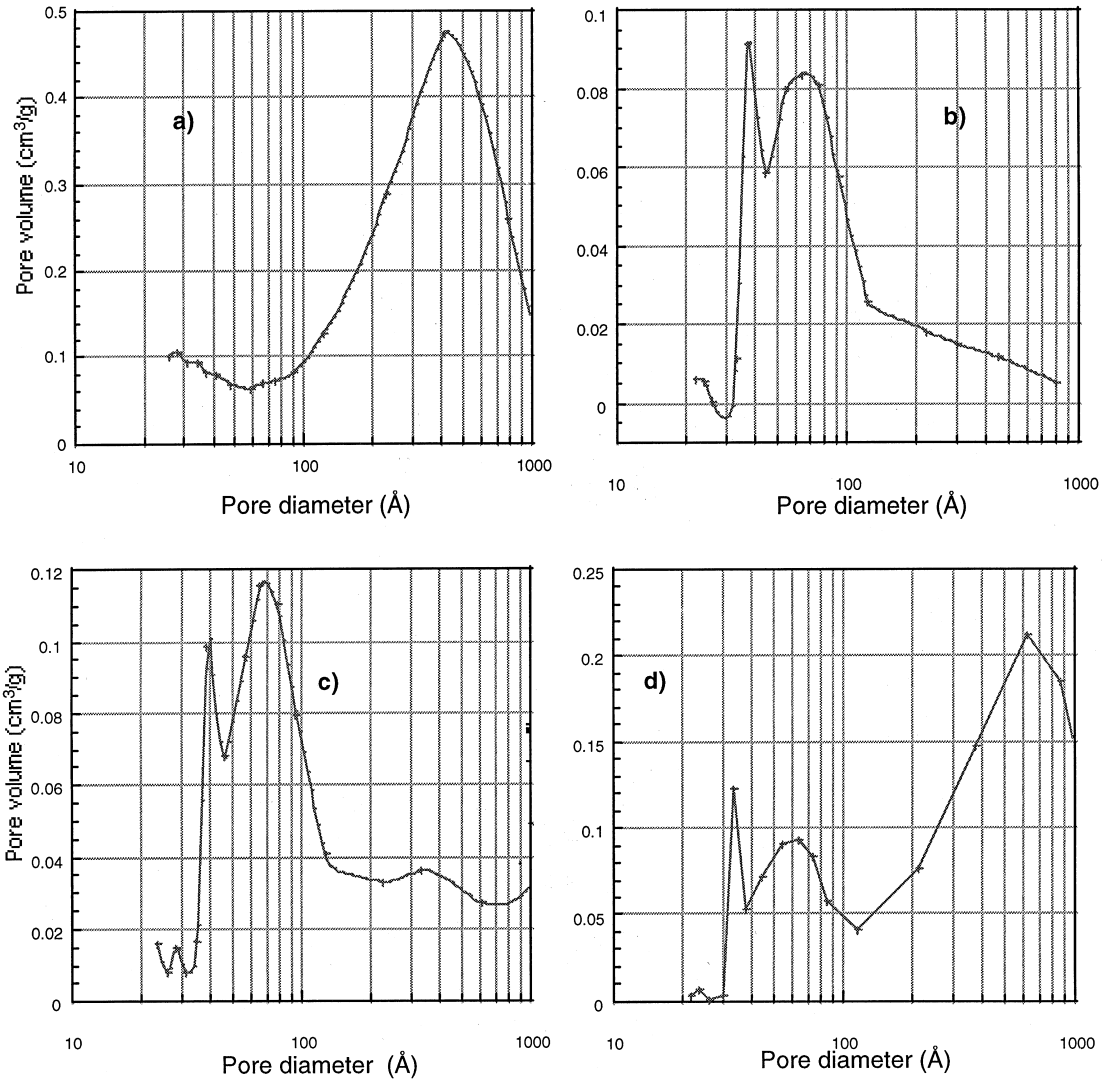

Fig. 5. Curves of pore size distribution of (a) carbon, (b) uranium trioxide, (c) (UO_3 + 3C) and (d) (UO_3 + 3C)* ground mixture.

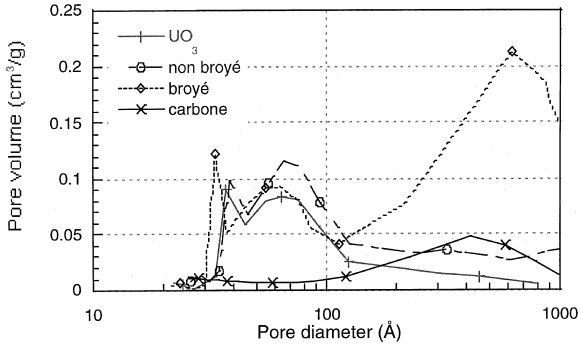

Fig. 6. Pore size distributions of all the samples, in which UO_3 and carbon are replotted in the scale corresponding to the amount of products used in the mixtures.

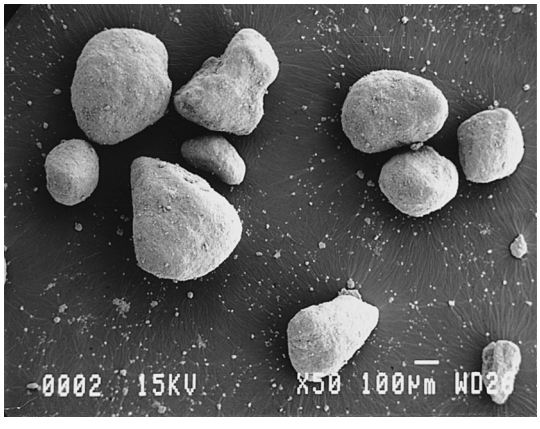

Fig. 7. SEM photograph of (UO_3 + 3C); magnification × 50.

Fig. 8. SEM photograph of $(UO_3 + 3C)^*$ ground mixture; magnification × 50.

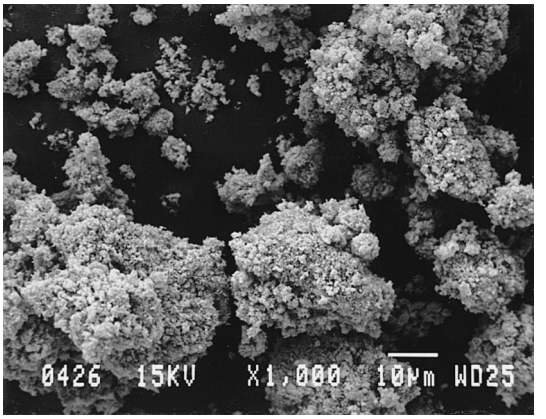

Fig. 10. SEM photograph of $(UO_3 + 3C)^*$ ground mixture; magnification × 1000.

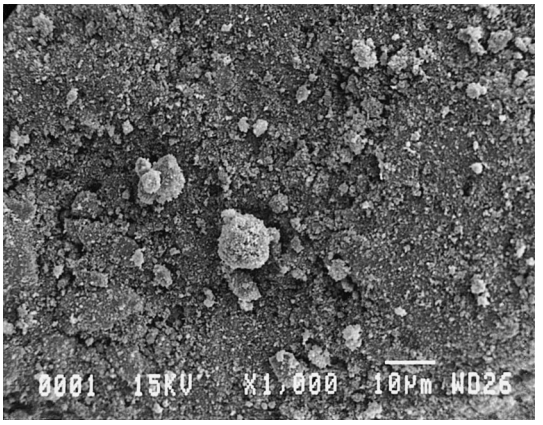

Fig. 9. SEM photograph of $(UO_3 + 3C)$; magnification × 1000.

accompanied by evolution of carbon dioxide and nitrogen dioxide (with appearance respectively of mass 44 and 46 to the mass spectrometer). The emission of nitrogen dioxide for each maximum is two orders of magnitude less in intensity than that of carbon dioxide, it does not contribute to the weight loss. The evolution of nitrogen dioxide during heating is probably due to the preparation method of uranium trioxide.

The DTG peak found at 823 K for the unground mixture (Fig. 14) presents the same maximum of temperature and weight loss (wt 1.8%) of the compound β-UO_3 (Fig. 13). So, this peak is attributed to the thermal decomposition of UO_3 into U_3O_8. Nevertheless, this DTG peak at 823 K found for the unground mixture disappears after grinding (Fig. 15) with higher weight losses at 713 and 863 K, respectively (2.3% instead of 0.6% for 713 K and 4.6% instead of 0.8% for 863 K). Moreover, we can notice for the $(UO_3 + 3C)^*$ ground mixture (Fig. 15) that the transformation is really completed at 1073 K with no more emission of carbon dioxide, whereas the unground mixture is not completely transformed even at 1173 K.

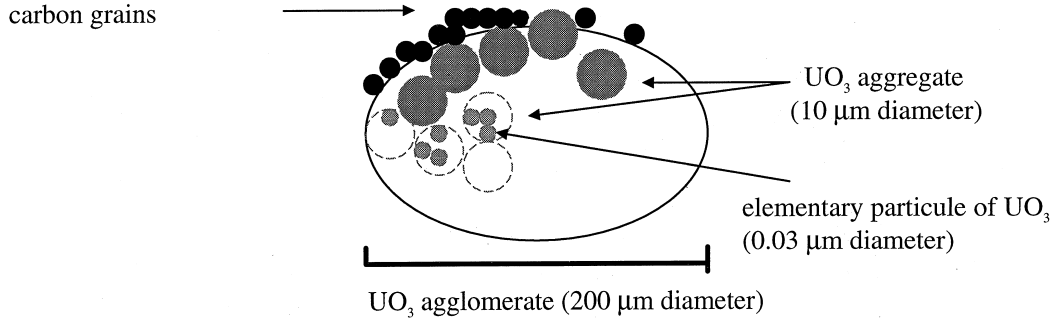

Fig. 11. Scheme of $(UO_3 + 3C)$ unground mixture.

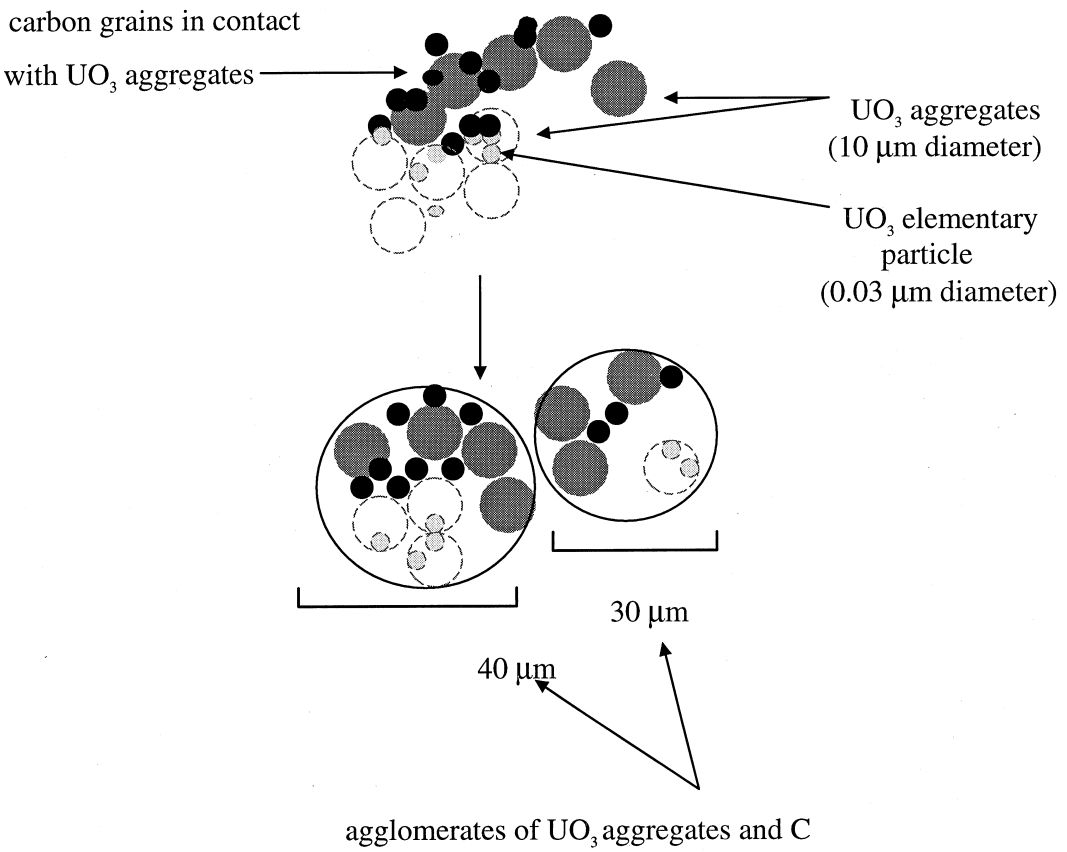

Fig. 12. Scheme of $(UO_3 + 3C)^*$ ground mixture.

The experimental weight loss (2.3%) observed for the ground mixture at 713 K is equivalent to the theoretical weight loss calculated for the reduction of UO_3 into U_3O_8 by carbon according to the reaction (3):

$$3(UO_3 + 3C) \rightarrow U_3O_8 + \frac{1}{2}CO_2 + \frac{17}{2}C. \quad (3)$$

And the 4.6% weight loss observed at 863 K for the ground mixture is similar to the theoretical value obtained for the reduction of U_3O_8 into UO_2 by carbon according to the reaction (4):

$$U_3O_8 + \frac{17}{2}C \rightarrow 3UO_2 + CO_2 + \frac{15}{2}C. \quad (4)$$

Besides, the XRD patterns of the products obtained at intermediate steps exhibit for the ground mixture (Fig. 16) only the peak of the U_3O_8 phase at 823 K and that of the UO_2 phase at 1173 K. Whereas, XRD patterns of the $(UO_3 + 3C)$ mixture given in Fig. 17, reveal the presence of two phases at 723 K, β-UO_3 and U_3O_8. We can observe only the U_3O_8 phase alone, after heating at 843 K. At 923 K, the UO_2 phase begins to appear but the U_3O_8 phase remains. At 1173 K the final product found is the UO_2 phase.

Consequently, from the results above we can interpret the TG and DTG curves of Figs. 14 and 15 as follows: reduction of UO_3 into U_3O_8 by carbon at 713 K, thermal decomposition of UO_3 into U_3O_8 at 823 K and carboreduction of U_3O_8 into UO_2 at 863 K.

These results are in agreement with the observation made by Mukerjee et al. [6]. Indeed, the temperature range of UO_3 thermal decomposition and UO_3 carboreduction into U_3O_8 are quite similar to those found by these authors under vacuum, with a temperature of carboreduction ($UO_3 \rightarrow U_3O_8$) always 100 K inferior to those required for thermal decomposition.

4. Discussion

For the carboreduction of U_3O_8 into UO_2, (the maximum of the DTG peak at 863 K) different mechanisms can be involved:

1. Diffusion of oxygen O from U_3O_8 to the surface carbon grains.

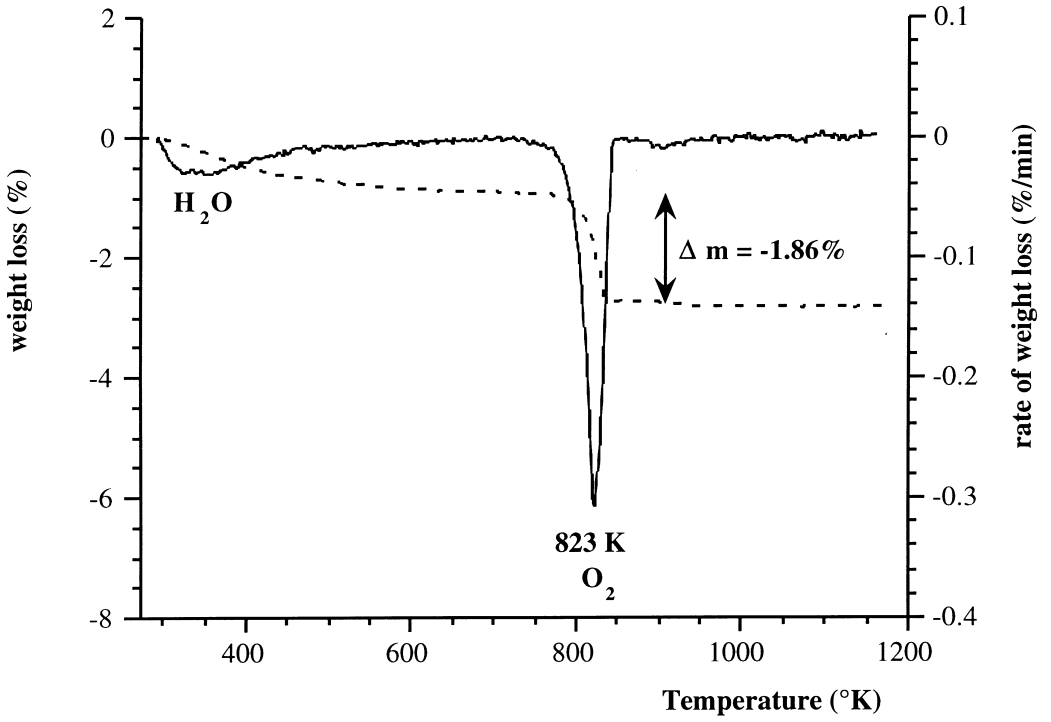

Fig. 13. (- - - -) weight loss and (–) rate of weight loss curves versus temperature for the β-UO_3 compound.

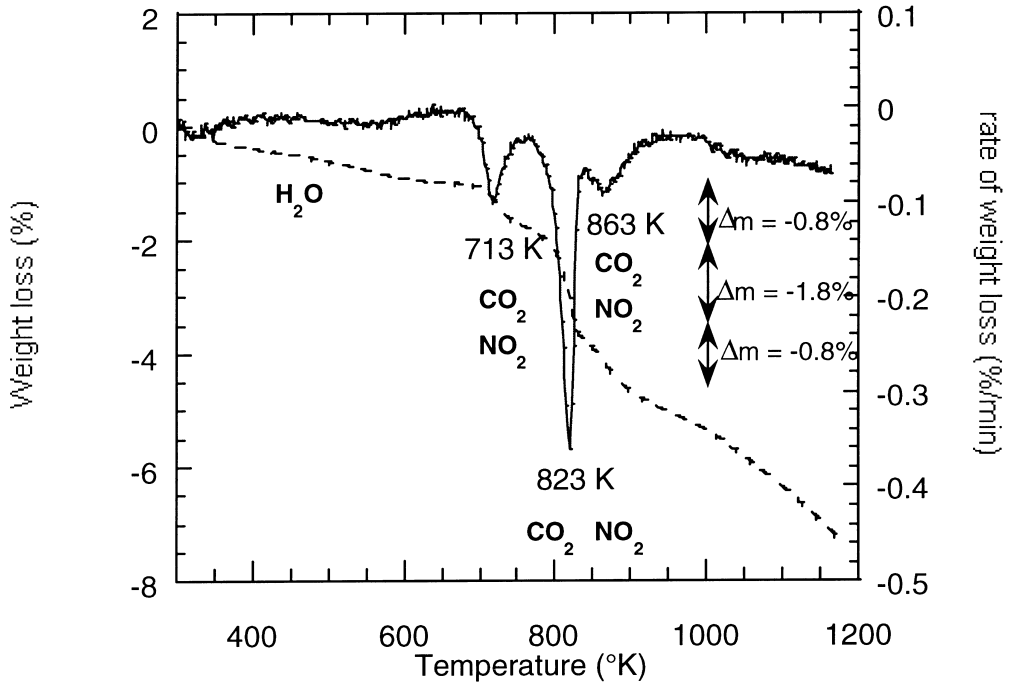

Fig. 14. (- - - -) weight loss and (–) rate of weight loss curves versus temperature for the (UO_3 + 3C) mixture.

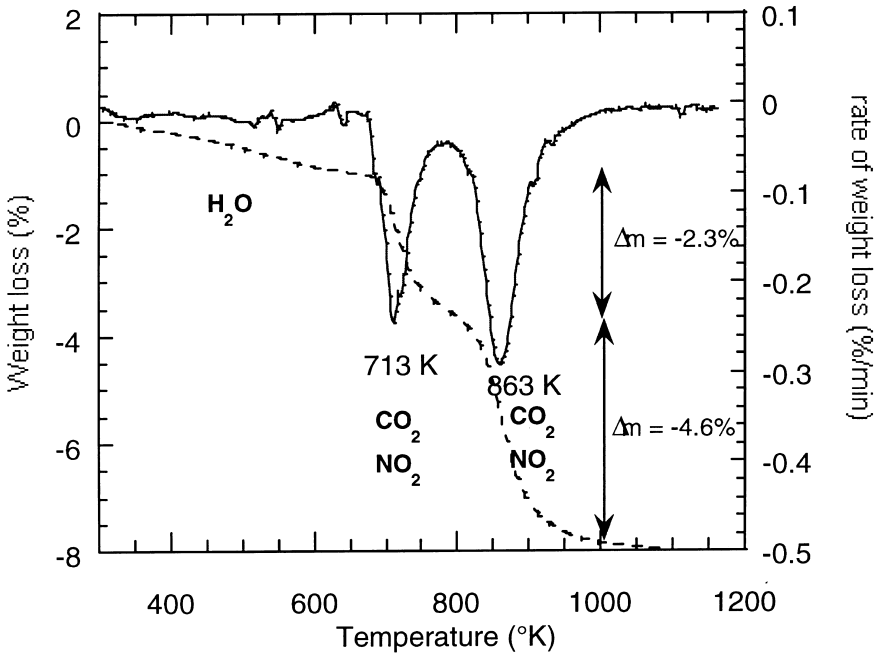

Fig. 15. (- - - -) weight loss and (–) rate of weight loss curves versus temperature for the $(UO_3 + 3C)^*$ ground mixture.

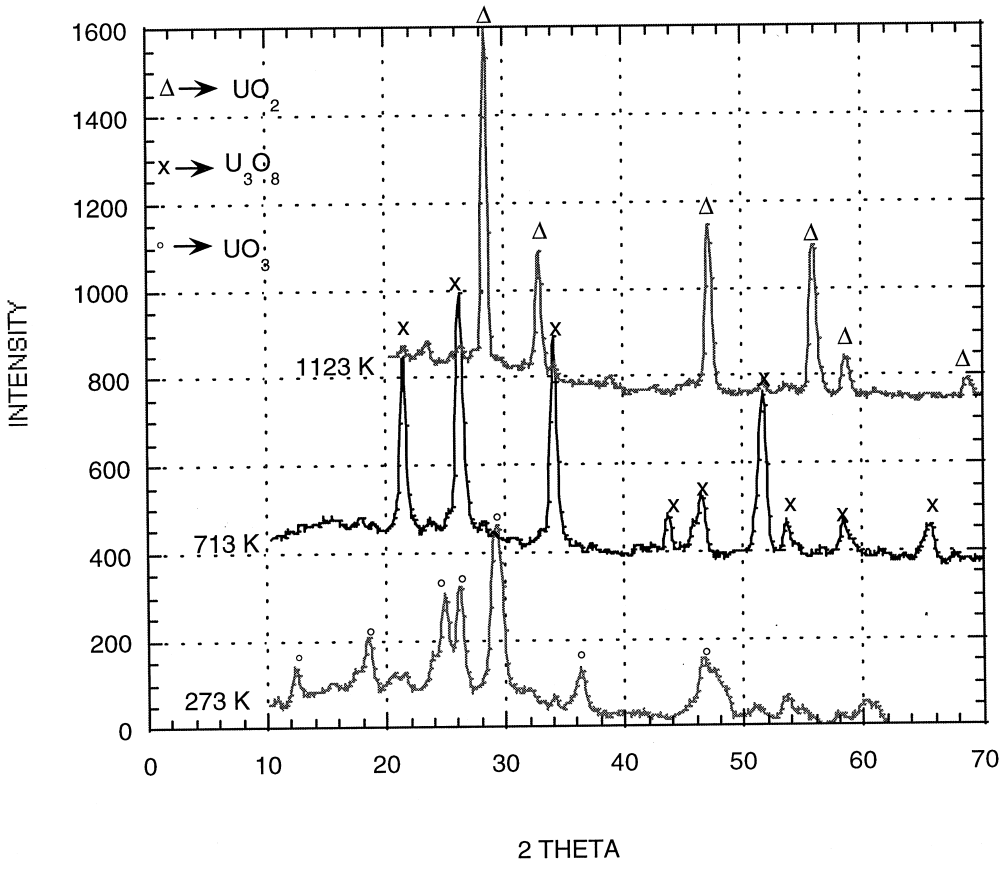

Fig. 16. The XRD patterns of the products obtained for the $(UO_3 + 3C)^*$ ground mixture at 273, 713, and 1123 K.

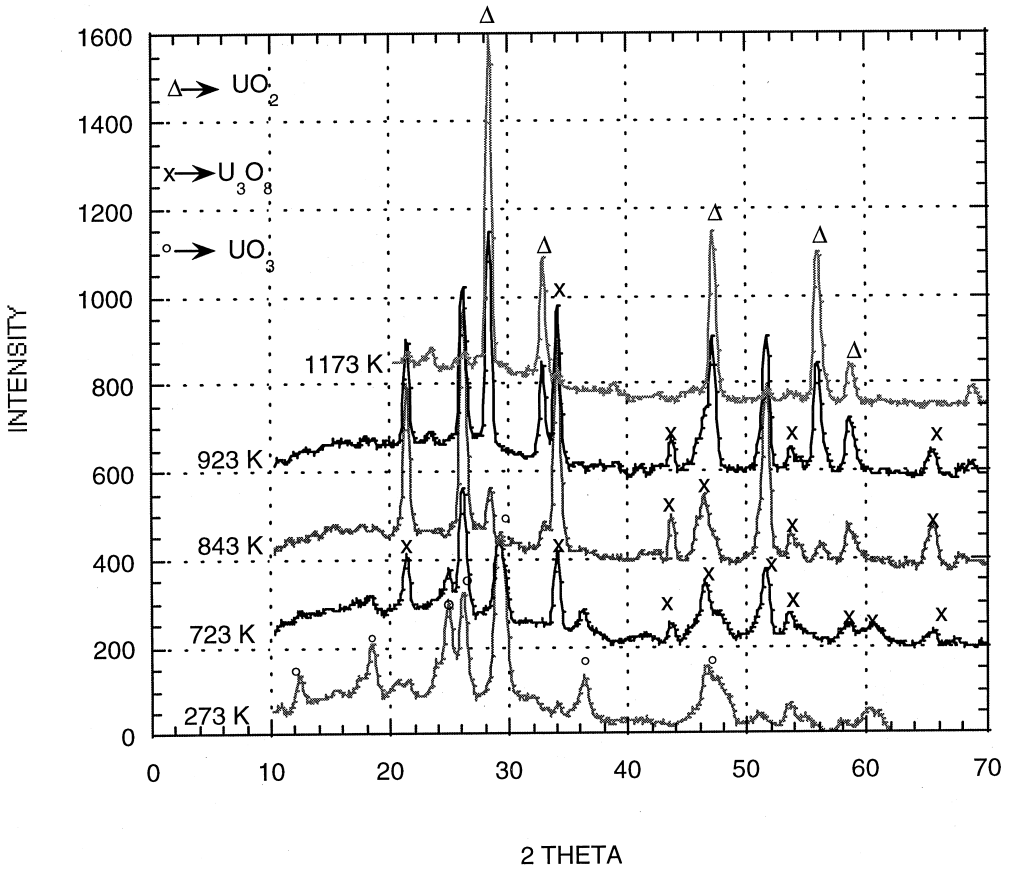

Fig. 17. The XRD patterns of the products obtained for the (UO_3 + 3C) unground mixture at 273, 723, 843, 923, and 1123 K.

2. Diffusion of carbon to the surface of the U_3O_8 particles.
3. Reduction by gaseous CO intermediate.

The fact that the reduction is completed at 1073 K for the ground mixture and uncompleted for the unground mixture, means that the contact between uranium oxides and carbon grains must be favored. Moreover, we have never detected CO during the carboreduction, although at temperatures higher than 1073 K it is possible to form CO gas according to the Boudouard equilibrium (5):

$$CO_2 + C = 2\,CO \quad (5)$$

So, we can consider that the U_3O_8 carboreduction involves a diffusion step (cases 1 and 2). The diffusion coefficients of oxygen or carbon are such that in the case of the unground mixture, only UO_3 particles nearest to carbon grains are first reduced.

Nevertheless, to decide about which of the oxygen or carbon is the diffusing species, it is necessary to complete this work by a kinetic study. Indeed, the absolute rate of conversion depends on the surface where the rate determining step occurs. This is being studied and will be dealt with in a forthcoming paper.

5. Conclusion

We have shown by SEM that the grinding increases the number of contacts between uranium trioxide aggregates and carbon by penetration of carbon grains inside new smaller agglomerates, formed during grinding. The consequence of the improvement of the contacts between the two reactants leads to a better behavior of the mixture during carboreduction, as clearly demonstrated by the TG study. Indeed, for the unground mixture the transformation of UO_3 into U_3O_8 is essentially realized by thermal decomposition (about 823 K). Only a few carbon grains participate in the reduction of UO_3 to U_3O_8 which certainly are the carbon grains surrounding the agglomerates, since only the carbon grains around the large agglomerates are in direct contact with the uranium oxides aggregates. Consequently, for the same reason, only a small proportion of U_3O_8 can be reduced to UO_2 by carbon at 863 K in this mixture. Whereas for the ground mixture, it is clear that all the UO_3 particles are reduced to U_3O_8 by carbon at 713 K, and the U_3O_8 particles formed are reduced to UO_2 at about 863 K by carbon. Contrary to the unground

mixture, the carboreduction of uranium trioxide to uranium dioxide is completed at 1073 K.

References

[1] L. Morrow, S.A. Graves, S. Tomlinson, Trans. Faraday Soc. 57 (1961) 1400.
[2] Tomlinson, Morrow, Graves, Trans. Faraday Soc. 57 (1961) 1008.
[3] R.M. Dell, V.J. Wheeler, Trans. Faraday Soc. 58 (1962) 1590.
[4] J.J. Katz, E. Rabinowitch, The Chemistry of Uranium, Part 1. Element, its Binary and Related Compounds, McGraw Hill, New York, 1951.
[5] J.J. Lawrence, D.J. O'Connor, J. Nucl. Mater 4 (1961) 79.
[6] S.K. Mukerjee, G.A.R. Rao, J.V. Dehadraya, V.N. Vaidya, V. Venugopal, D.D. Sood, J. Nucl. Mater. 199 (1993) 247.